[^{18}F]VUIIS1009B Features a Superior Imaging Performance to [^{18}F]DPA-714 in TSPO Density Characterization for Neuroinflammatory PET Imaging

Chen Huang
Shanghai University of Medicine and Health Sciences
Fan Ding
Shanghai Jiao Tong University School of Medicine
Yong Hao
Shanghai Jiao Tong University School of Medicine
Zhoumi Hu
Shanghai Jiao Tong University School of Medicine
Cheng Wang
Shanghai Jiao Tong University School of Medicine
Wei Li
Shanghai University of Medicine and Health Sciences
Mengxin Wang
Shanghai University of Medicine and Health Sciences
Wenxian Peng
Shanghai University of Medicine and Health Sciences
Dewei Tang (acetdw@126.com)
Shanghai Jiao Tong University School of Medicine https://orcid.org/0000-0002-5427-9671

Original research

Keywords: Translocator Protein (TSPO), DPA-714, VUIIS1009A, VUIIS1009B, parametric image, binding potential, total distribution volume

Posted Date: September 11th, 2020

DOI: https://doi.org/10.21203/rs.3.rs-39569/v2

Abstract

Purpose: Translocator protein (TSPO), an outer mitochondrial membrane protein, is regarded as a key biomarker for neuroinflammation in a variety of neurodegenerative diseases. In this study, we aim to evaluate two highly specific TSPO radiotracers [^{18}F]VUIIS1009A and [^{18}F]VUIIS1009B in a mild cerebral ischemic rat model, and to compare their *in vivo* performance to the well-established TSPO probe [^{18}F]DPA-714 for neuroinflammation imaging. With multiple graphic analytical methods tested and macro parameters determined, we propose to find a suitable and best quantification method to profile neuroinflammation and measure TSPO density with the three TSPO radiotracers.

Methods: Cerebral ischemia rat model was created and imaged using [^{18}F]VUIIS1009A, [^{18}F]VUIIS1009B and [^{18}F]DPA-714. Displacement studies using non-radioactive analogs were performed to evaluate the binding specificities of [^{18}F]VUIIS1009A and [^{18}F]VUIIS1009B individually. Imaging analysis using arterial plasma input functions (AIFs) was employed to generate Logan plots and parametric images of total distribution volume (V_T) for each radiotracer. Reference Logan model using contralateral brain as a reference region was introduced to generate parametric images for binding potential (BP_{ND}).

Results: When compared to [^{18}F]DPA-714, [^{18}F]VUIIS1009B demonstrated higher binding potential (BP_{ND}) and distribution volume ratio (DVR). Parameter images of BP_{ND} and V_T also indicate [^{18}F]VUIIS1009B has a superior imaging profile with higher BP_{ND} and DVR when compared with other two radiotracers in TSPO imaging. Correlation analysis between BP_{ND} for [^{18}F]VUIIS1009B and [^{18}F]DPA-714 also indicates [^{18}F]VUIIS1009B is more sensitive than [^{18}F]DPA-714 in TSPO density measurement.

Conclusions: This study demonstrates the superiority of [^{18}F]VUIIS1009B to [^{18}F]VUIIS1009A and [^{18}F]DPA-714 in the neuroinflammation imaging. It also demonstrates that [^{18}F]VUIIS1009B PET imaging coupled with parameter mapping (V_T and BP_{ND}) and graphic analysis using Logan analysis and reference Logan analysis holds great promise for neuroinflammation characterization and TSPO density measurement.

Introduction

Neuroinflammation, as a response to local insult or the distally existing pathological events in central nervous system (CNS), often occurs in a variety of neurological disease states, including Alzheimer's diseases (AD), Parkinson's disease (PD), multiple sclerosis (MS), Huntington's disease (HD), and amyotrophic lateral sclerosis (ALS) [1-4]. Neuroinflammation often plays an important role in various neuropathologies. Neuroinflammation targeted diagnosis and therapy are often regarded to be crucial for disease progress monitoring and novel therapy evaluation [5]. Among those studies, neuroimaging provides a non-invasive tool to characterize and monitor *in vivo* neuroinflammation. As one of the neuroimaging modalities, positron emission tomography (PET) can be employed to visualize and quantify the target at nanomolar level, with both high sensitivity and specificity.

Translocator protein (TSPO, 18 kDa), one of the most popular PET imaging biomarkers for neuroinflammation, has been studied in neuroinflammation for over 20 years[6]. As an outer mitochondrial membrane protein, TSPO has an extremely low expression level in healthy brain[7], but an overexpression when microglia are activated in neuroinflammation in response to brain injury[5]. Overexpression of TSPO is considered as a biomarker for neuroinflammation in numerous neurological diseases including stroke, AD, PD, MS, HD, and ALS[7]. Development of TSPO-PET imaging was characterized by the discovery of many novel TSPO radiotracers [5], including the most common radiotracer [^{11}C]PK11195[6], phenoxyarylacetamides derivatives ([^{11}C]DAA1106, [^{11}C]PBR28, [^{18}F]FEDAA1106, [^{18}F]FEPPA, [^{18}F]PBR06), imidazopyridines derivatives ([^{11}C]CLINME), and pyrazolopyrimidines derivatives ([^{18}F]DPA-714) [8]. Among these, [^{18}F]DPA-714 is a pyrazolopyrimidinal radiotracer featuring a high TSPO binding affinity (**Figure 1**) [9] [10]. Labeled with ^{18}F, [^{18}F]DPA-714 also has a longer half-time (110 min) than [^{11}C]PK11195 (20 min). Clinical studies using [^{18}F]DPA-714 have been performed on patients with ALS[11] [12], AD [12] [13], as well as in post-stroke studies[14], with great promise demonstrated in neuroimaging.

Based on the scaffold of [^{18}F]DPA-714, many novel radiotracers have been developed and introduced in both clinical and preclinical studies, including [^{18}F]DPA-C5yne[15], [^{18}F]VUIIS1008[16-17], [^{18}F]VUIIS1009A/B[18], [^{18}F]FDPA[19], [^{18}F]VUIIS1018A[20-21]. Of these radiotracers, [^{18}F]VUIIS1009A and [^{18}F]VUIIS1009B demonstrate over 500-fold higher binding affinities when compared to the parent radiotracer [^{18}F]DPA-714[18]. Imaging with these two radiotracers in C6 glioma model also demonstrates the superiority of [^{18}F]VUIIS1009B to [^{18}F]VUIIS1009A and [^{18}F]DPA-714, including higher BP_{ND}, higher SNR and higher distribution volume ratio (DVR)[18].

Although TSPO PET imaging has been performed in a variety of neuroinflammatory diseases, it still has some drawbacks, including relatively low neuroinflammatory uptake, low SNR and insensitivity to the small variance of TSPO expression when quantified with the semi-quantitative parameters (%ID/cc or SUV) [22]. In order to overcome these limitations, macro parameters like V_T, BP_{ND} and DVR were often introduced to TSPO imaging, with the aim to fully characterize radiotracer pharmacokinetics, TSPO expression level, as well as to increase SNR and to improve imaging visual effects [23] [22, 24-26]. In practice, radiotracers featuring higher binding specificity often demonstrate higher macro parameter values (like BP_{ND}), higher SNR and thus better visual effects in PET imaging as well as the higher sensitivity to TSPO density variance. Considering this, in this study, for the first time we evaluated the performance of the highly specific TSPO radiotracers [^{18}F]VUIIS1009A and [^{18}F]VUIIS1009B with directly comparison to the performance of [^{18}F]DPA-714 in a mild neuroinflammation model. As shown in **Figure 1**, VUIIS1009A (IC_{50}: 14.4 pM) features a 750-fold higher *in vitro* TSPO binding affinity than DPA-714 (IC_{50}: 10.9 nM)[27]. VUIIS1009B (IC_{50}: 19.4 pM) features a 560-fold higher *in vitro* TSPO binding affinity than DPA-714. With *in vivo* PET dynamic scans, we evaluated their semi-quantitative parameters (%ID/cc or SUV), as well as macro parameters including binding potential (BP_{ND}), total distribution volumes (V_T)

and distribution volume ratio (DVR). Specific parametric images (BP_{ND}, V_T) were also generated and compared to identify the suitable quantitative methods and parameters to profile neuroinflammation in this study.

Materials And Methods

ll chemicals were purchased from commercial sources. Unlabeled DPA-714, VUIIS1009A/B and their precursor for radiosynthesis were synthesized in-house, and ^{18}F was produced using an IBA cyclotron (Belgium). Effluent radioactivity was monitored using a NaI (Tl) scintillation detector system. All other synthesis reagents and solvents were purchased from Sigma-Aldrich (St. Louis, MO, USA) and used without further purification, unless noted otherwise.

Radiosynthesis. Radiosynthesis of probe [^{18}F]DPA-714, [^{18}F]VUIIS1009A and [^{18}F]VUIIS1009B was performed according to our previously published methods [18, 28]. In detail, precursors underwent nucleophilic fluorination with fluorine-18. Purification of ^{18}F-labeled radiotracers was performed with preparative HPLC. The retention time of all the radiotracers according to gamma detection was double checked to make sure it was in agreement with the UV retention time, which was determined using the corresponding non-radioactive analogs under the same condition for HPLC analysis. The radiochemical purity measured using HPLC was consistently greater than 99 %, with specific activity consistently greater than 4203 Ci/mmol (156 TBq/mmol).

Animals. Animals were maintained and handled in accordance with the recommendations of the National Institute of Health in China. Animal studies were approved by the local University and Hospital Ethics Committee. All experiments conducted at the Shanghai Jiao Tong University School of Medicine were approved by the Animal Ethics Committee. Male Wistar rats (n = 9, 7 weeks old, 230 - 250 g) were purchased from Vital River (Beijing, China) and housed under a 12-h/12-h dark/light cycle under optimal conditions.

Ischemia Rat Models. Mild focal ischemia was induced by intraluminal occlusion of the middle cerebral artery for 30 min based on the intraluminal thread model[29]. After ischemic surgery, the rats were used for PET imaging, and metabolite analysis at 5 - 7 days. Rats (n = 9) were affixed with arterial catheters prior to the PET/CT studies. Of the 9 animals, 6 rats were used repeatedly for PET imaging using the three individual radiotracers, 3 for repeatable displacement studies with [^{18}F]VUIIS1009A and [^{18}F]VUIIS1009B, with a total of 24 PET scans performed in this study. We chose 5-7 days for PET imaging with the aim to image the early stage of neuroinflammation instead of the advanced stage with maximal uptake. This early stage imaging is meaningful to early detection of neuroinflammation. Moreover, in the early stage of neuroinflammation, contralateral brain should have little or tiny expression of TSPO, which will benefit the following graphic analysis using it as the reference region.

***In Vivo* Dynamic PET Imaging Study.** PET imaging was carried out using a small-animal PET scanner (Siemens Medical Solutions USA, Knoxville, TN, USA) according to the protocols reported previously[9].

Rats (n = 6) were first anesthetised with isoflurane (3.5% for induction, 1.5–2% for maintenance). Immediately after rats were intravenously injected *via* the tail vein with specific radiotracers, a 45-min list-mode emission scan was conducted immediately. The study was performed using [^{18}F]VUIIS1009A (46.0 ± 8.0 MBq), [^{18}F]VUIIS1009B (48.8 ± 10.7 MBq) and [^{18}F]DPA-714 (47.2 ± 9.9 MBq) in consecutive days. During the scans, blood samples were drawn according to the following schedule: 15 µl every 10 s for the first 90 s and at 2, 5, 8, 12, 20, and 45 min. The time frame reconstruction for PET was as follows: 10s × 12 frames, 1 min × 3 frames, 5 min × 8 frames. In addition, the metabolite-corrected parent plasma input function (AIF) was measured according to our previous published protocol[17-18] .

For the displacement experiments, unlabeled TSPO compounds VUIIS1009A (10.0 mg/kg) or VUIIS1009B (10.0 mg/kg) were dissolved in 1.0 mL of saline containing 10% ethanol and 5% Tween-80, and injected 20 min after the PET scans were initiated. In this study, the same cohort of rats (n = 3) were imaged and evaluated for each radiotracer individually. Dynamic image reconstruction was achieved by filtered back-projection using Hanning's filter with a Nyquist cutoff frequency of 0.5 cycles/pixel.

PET Image Co-registration

In order to analyze the voxel values of the regions of interest (ROI) and calculate the parametric maps, PET images of the same rat with different radiotracers were co-registered. In detail, using Inveon Research Workplace 4.0 (Siemens Medical Solutions USA, Knoxville, TN, USA), corresponding CT images were first co-registered to make the spatial alignment of brain regions. The transformation file for this co-registration was generated and then treated as an input to register the corresponding PET images. With the registered PET images, ROIs of ipsilateral and contralateral brain were drawn and values of voxels was analyzed.

Dynamic PET Data Analysis

The PET images were analyzed using PMOD version 3.4 image analysis software (PMOD Technologies, Zurich, Switzerland) and Inveon Research Workplace 4.0 (Siemens Medical Solutions USA, Knoxville, TN, USA). Regions of interest (ROIs) were manually defined for each rat on the region of increased radiotracer binding in the ipsilateral hemisphere. The ROIs were manually drawn on ipsilateral and contralateral brain as shown in **Figure 2** and **Figure 3**.

In this study, parametric V_T images were generated using plasma input-based Logan analysis[30], with the plasma contribution factor v_p set to 0.05 for all the analysis. With the same animals, parametric BP_{ND} images were also generated using Logan Reference Tissue model with contralateral brain TACs as an input [30]. For $DVR_{LoganRef}$ or BP_{ND} determination and parametric image generation, k_{2_REF} was calculated using SRTM methods with contralateral brain TACs input as the reference tissue [31]. DVR_{Logan} from the **Table 1** was generated directly from the ratio of distribution volume of ipsilateral and contralateral brain generated *via* the plasma input-based Logan analysis.

Statistical Analyses. All quantitative data are expressed as the mean ± standard deviation (SD).

Pearson's correlation analysis was applied to investigate the relationship between different parameters (V_T, BP_{ND}, %ID/cc *et al*) both at the voxel level and regional level, using GraphPad Prism 5 software (GraphPad Software, La Jolla, CA, USA).

Results

***In Vivo* 45-min Dynamic Scan.** Performance of [^{18}F]DPA-714, [^{18}F]VUIIS1009A and [^{18}F]VUIIS1009B was evaluated during the 45-min dynamic PET scan using a focal cerebral ischemic rat model, in which TSPO expression was up-regulated with activated microglia, whereas the blood-brain barrier (BBB) was intact or not seriously disrupted[32]. As expected, the ipsilateral side (ischemia side) showed a higher uptake of the radiotracer than the contralateral brain in the PET imaging for all of the three radiotracers, as shown in **Figure 2a**, **2b** for [^{18}F]DPA-714, **Figure 2c**, **2d** for [^{18}F]VUIIS1009A and **Figure 2e**, **2f** for [^{18}F]VUIIS1009B. A fast uptake of the radiotracers was demonstrated according to the analysis of time-activity curves (TACs) on the ipsilateral side (**Figure 2g** for [^{18}F]DPA-714, **Figure 2h** for [^{18}F]VUIIS1009A and **Figure 2i** for [^{18}F]VUIIS1009B). Moreover, consistent levels of radiotracer uptake on the ipsilateral side were achieved 2 min after the radiotracer injection as indicated by TACs (**Figure 2g** for [^{18}F]DPA-714, **Figure 2h** for [^{18}F]VUIIS1009A and **Figure 2i** for [^{18}F]VUIIS1009). TACs for corrected AIFs was also shown in **Supplemental Figure 1.** Compared to [^{18}F]DPA-714 (%ID/cc = 0.73 ± 0.08 at 45 min), [^{18}F]VUIIS1009B (%ID/cc = 0.70 ± 0.05 at 45 min) has a comparable %ID/cc in the ipsilateral region, while [^{18}F]VUIIS1009A (%ID/cc = 0.50 ± 0.05 at 45 min) has a significantly lower uptake in the same region as shown in **Figure 2c, 2d** and **2h**.

The contralateral brain had a comparatively low uptake, and a consistent %ID/cc level was achieved at 10 min after the radiotracer injection for all three radiotracers (**Figure 2g**, **Figure 2h** and **Figure 2i**). When compared to [^{18}F]VUIIS1009A, [^{18}F]VUIIS1009B and [^{18}F]DPA-714 demonstrate a higher contralateral brain uptake as indicated in the 45 min uptake (0.20 ± 0.03 *vs* 0.15 ± 0.01, ID%/cc at 45 min). For [^{18}F]DPA-714, the %ID/cc ratio at 45 min between the ipsilateral brain and contralateral brain in this study was 3.50 as shown in the TACs (0.73 ± 0.08 vs. 0.20 ± 0.03 %ID/cc at 45 min; **Figure 2g**), 3.33 for [^{18}F]VUIIS1009A (0.50 ± 0.05 vs. 0.15 ± 0.01 %ID/cc at 45 min) and 3.50 for [^{18}F]VUIIS1009B (0.70 ± 0.05 vs. 0.2 ± 0.03 %ID/cc at 45 min), indicating a high and comparable signal-to-noise ratio of all the three TSPO radiotracers in this study.

***In Vivo* Displacement Study.** [^{19}F]VUIIS1009A and [^{19}F]VUIIS1009B were used for the displacement assay and were injected at 20 min in the course of a 45-min dynamic scan. Based on the imaging results, both TSPO compounds could displace the radioactivity uptake on the ipsilateral side of the brain. As shown in **Figure 3a**([^{18}F]VUIIS1009A) and **3c**([^{18}F]VUIIS1009B), the uptake on the ipsilateral side was significantly higher than the uptake on the contralateral brain for both radiotracers before the injection of their non-radioactive analogs. However, after the displacement, radiotracer uptake of the ipsilateral brain dropped

dramatically (**Figure 3b** and **3d**), which accounts to more than 66% decrease of the tracer uptake when compared to the normal uptake in the same intervals as shown in the TACs for both radiotracers (as shown in **Figure 2g, 2h, 3e** and **3f**). This is similar to the displacement ratio reported by Martin et al on [^{18}F]DPA-714 displacement study with the same ischemia animal model[33]. After displaced with their non-radioactive analogs, the uptake level of ipsilateral brain was almost comparable to the contralateral brain, both demonstrated by the imaging profiles and TACs in **Figure 3**. All these indicate the significantly high binding specificity for both radiotracers in ipsilateral brain.

Macro Parameters Determined using Graphic Analysis

Although both [^{18}F]VUIIS1009A and [^{18}F]VUIIS1009B have significantly higher *in vitro* binding affinities when compared to [^{18}F]DPA-714, they did not demonstrate a more promising imaging characterized by the semi-quantitative uptakes (like %ID/cc) as shown in **Figure 2**. In order to further evaluate their *in vivo* performances, macro parameters like V_T, DVR and BP_{ND} were determined using graphic analysis with AIFs or reference tissue TACs input. According to our previous studies, TSPO PET imaging can be analyzed using a two-tissue, four-parameter model[9, 18, 20](model fit as shown in **Supplemental Figure 2**). In this study, graphic analysis using AIFs can also be employed to determine the V_T for both ipsilateral and contralateral brain region. As shown in **Table 1**, V_T determined for ipsilateral region are higher than the corresponding values for contralateral brain for all the three radiotracers, indicating all these radiotracers tend to accumulate in ipsilateral region instead of the contralateral brain. Direct comparison of the ipsilateral V_T from three radiotracers indicates [^{18}F]VUIIS1009B has a higher V_T than the other two radiotracers as shown in **Table 1**. Moreover, for the contralateral brain, [^{18}F]VUIIS1009B also demonstrates a slightly higher V_T than the other two radiotracers. The ratios of the V_T values (noted as DVR_{Logan}) between ipsilateral brain and contralateral brain indicate a higher DVR_{Logan} for [^{18}F]VUIIS1009B (8.53 ± 1.06) when compared with [^{18}F]DPA-714 (6.00 ± 0.41) and [^{18}F]VUIIS1009A (4.37 ± 0.82). Further study using contralateral brain as a reference region was also performed to determine $DVR_{LoganRef}$ and BP_{ND} for all three radiotracers (as shown in **Figure 4** and **Table 1**). Logan plots using contralateral brain as a reference region was plotted with BP_{ND} and $DVR_{LoganRef}$ determined (**Figure 4a, 4b and 4c)**, demonstrating a good fit and linearity for all three radiotracers with $r > 0.96$. As shown in **Table 1**, [^{18}F]VUIIS1009B (7.55 ± 0.65) demonstrating a much higher $DVR_{LoganRef}$ than [^{18}F]DPA-714 (5.37 ± 0.36) and [^{18}F]VUIIS1009A (3.91 ± 0.50). Similarly, [^{18}F]VUIIS1009B also demonstrates a much higher BP_{ND} value than other two radiotracers as shown in **Table 1**. In sum, the macro parameter analysis revealed that [^{18}F]VUIIS1009B has a superior imaging potential than the other two radiotracers on V_T, DVR and BP_{ND}.

Parametric Image Analysis

Macro parameter analysis using Logan plot revealed [^{18}F]VUIIS1009B is superior to [^{18}F]DPA-714 and [^{18}F]VUIIS1009A as shown in dynamic PET imaging. In this study, we further compared the performance

of the three radiotracers using parameter images (V_T and BP_{ND}) generated (**Figure 5**). In detail, voxel-wise V_T images were generated *via* a Logan graphic method using AIFs. Voxel-wise BP_{ND} images were generated using a Logan reference model with the contralateral brain input as the reference region. As expected, compared to [^{18}F]DPA-714, [^{18}F]VUIIS1009B has similar biodistribution profile for both V_T and BP_{ND} parameter images (**Figure 5**), but features higher DVR, BP_{ND} in the ipsilateral region, demonstrating its promising characteristics for TSPO imaging. Interestingly, although [^{18}F]VUIIS1009A and [^{18}F]VUIIS1009B feature the comparably high *in vitro* binding affinity, [^{18}F]VUIIS1009A did not show a similar imaging profile as [^{18}F]VUIIS1009B in both V_T and BP_{ND} parametric images (**Figure 5**). Compared to the parametric image of [^{18}F]VUIIS1009B, [^{18}F]VUIIS1009A imaging analysis generated a noisier parametric image as shown in **Figure 3a** and **Figure 3b**. The distribution for [^{18}F]VUIIS1009A V_T image does not match the %ID/cc image of [^{18}F]VUIIS1009A as shown in **Figure 2C**, as well as the other images for [^{18}F]DPA-714 and [^{18}F]VUIIS1009B as shown in **Figure 2** and **Figure 5**, indicating a poor visual quality for [^{18}F]VUIIS1009A imaging when compared to other two radiotracers.

Correlation between %ID/cc, BP_{ND} and V_T at the Voxel Level

This study also determined and evaluated %ID/cc, BP_{ND} and V_T at the voxel level, with the aim to better elucidate the relationship among these parameters derived from the dynamic PET images. As shown in **Figure 6**, with %ID/cc, BP_{ND} and V_T determined for the voxels in the ipsilateral brain, we made different plots for the three probes and measured the correlation coefficient *r* and *p* value for each data set. As shown in **Figure 6a** and **6c**, a strong correlation was elucidated for [^{18}F]DPA-714, [^{18}F]VUIIS1009B among all three parameters (%ID/cc, BP_{ND} and V_T). Compared to [^{18}F]DPA-714, [^{18}F]VUIIS1009B demonstrates a higher *r* value (0.99 *vs.* 0.78) and thus a more positive linear relationship between V_T and BP_{ND} as shown in **Figure 6a** and **6c**. Furthermore, [^{18}F]VUIIS1009B also demonstrates a stronger correlation between semi-quantitative parameter %ID/cc and BP_{ND} or V_T, as shown by the plots in **Figure 6a** and **6c**, which is probably due to the lower non-specific binding profile for [^{18}F]VUIIS1009B instead of [^{18}F]DPA-714. While for [^{18}F]VUIIS1009A, a weaker correlation is found between %ID/cc and the other two parameters (BP_{ND} and V_T) as shown in **Figure 6b**.

Correlation Analysis between BP_{ND} for [^{18}F]VUIIS1009B and [^{18}F]DPA-714

In this study, both [^{18}F]VUIIS1009B and [^{18}F]DPA-714 PET imaging were performed using the same rats with the aim to more accurately reflect their BP_{ND} and *in vivo* performance. In order to compare the performance of [^{18}F]VUIIS1009B and [^{18}F]DPA-714, we co-registered the PET images from the same rats and calculated BP_{ND} for [^{18}F]VUIIS1009B and [^{18}F]DPA-714 both at the regional level and voxel level with the same ROIs. As shown in **Figure 7a**, [^{18}F]VUIIS1009B demonstrates a strong positive correlation with [^{18}F]DPA-714 (r = 0.88) at the voxel level in the same rat. The slope of the fitting curve is 1.35, which indicate the BP_{ND} for [^{18}F]VUIIS1009B is more sensitive to TSPO expression when compared to [^{18}F]DPA-

714. Regional BP_{ND} was also obtained and analyzed for both [^{18}F]VUIIS1009B and [^{18}F]DPA-714 for the same rats (n = 6). As shown in **Figure 7b**, [^{18}F]VUIIS1009B also demonstrates a stronger correlation of [^{18}F]DPA-714 in the regional BP_{ND} (r = 0.89) for a cohort of rats (n = 6). The slope for the fitting curve is 1.45, which also demonstrates the higher sensitivity of [^{18}F]VUIIS1009B to profile TSPO expression when compared to [^{18}F]DPA-714.

Discussion

With a low expression in normal brain, TSPO is normally overexpressed in neuropathological conditions, such as stroke, brain trauma, AD, and PD. TSPO PET imaging is now becoming a useful tool in neuroinflammation evaluation, as well as in diagnosis and therapy evaluation for many neurological diseases. In the longitudinal studies of neurological diseases, TSPO density evaluation with different radiotracers and analytical approaches have been performed to increase the sensitivity of TSPO expression characterization, and thus to elucidate the relationship between the disease progression and TSPO density [34-37]. In these studies, semi-quantitative parameters like %ID/cc and SUV are widely evaluated in both clinical and preclinical studies[33, 38]. Compared to the semi-quantitative parameters, macro parameters (like BP_{ND}, DVR, V_T) can provide more detailed information on radiotracer pharmacokinetics and TSPO expression, which is more meaningful in longitudinal monitoring of neuroinflammatory diseases [39]. Moreover, TSPO radiotracers with higher binding affinities tend to have higher binding potential (BP_{ND}), which can be more sensitive to measure the variance of TSPO densities in the longitudinal analysis of disease progression. [^{18}F]DPA-714, a second-generation radiotracer developed by James *et al.*[10], demonstrated its superiority in neuroinflammation imaging, with higher binding potential, binding specificity and SNR. Martin *et al* performed the [^{18}F]DPA-714 PET imaging to determine the time course of TSPO expression over several days in a focal cerebral ischemia model of rat. In this study, the *in vivo* PET imaging and *in vitro* autoradiographic results confirmed increase in [^{18}F]DPA-714 binding at 4 and 7 days after cerebral ischemia, reaching a maximal value at 11 days, followed by slow return to normal values at 30 days. This study also demonstrated that [^{18}F]DPA-714 provides accurate informative information of the expression and distribution of TSPO activity after cerebral ischemia[33]. Similarly, Pulagam *et al* also demonstrated the feasibility to use [^{18}F]VUIIS1008 to monitor TSPO expression longitudinally in a rat model of cerebral ischemia, with the results suggesting ^{18}F-VUIIS1008 could become a valuable tool for the diagnosis and treatment evaluation of neuroinflammation following ischemic stroke[38]. Furthermore, Golla *et al.* used multiple methods to generate the quantitative images for [^{18}F]DPA-714 in a clinic study with healthy subjects and AD patients participated [40]. In this study, they concluded that both Logan analysis and spectral analysis are suitable plasma input–based methods to generate quantitatively accurate parametric V_T images. Meanwhile, in reference tissue approaches, reference Logan analysis or SRTM2 can be used to generate parametric BP_{ND} images [40].

In our previous studies, we further modified [^{18}F]DPA-714 and discovered several novel TSPO imaging radiotracers, including [^{18}F]VUIIS1008 [16-17], [^{18}F]VUIIS1018A [20-21] and [^{18}F]VUIIS1009A/B [18]. These novel radiotracers feature higher *in vitro* TSPO binding affinities and suitable lipophilicities for brain imaging, when compared to the parent radiotracer [^{18}F]DPA-714. Moreover, they also demonstrated great potential in TSPO PET imaging, including high SNR, higher binding potential, and enhanced visual effects[16-18]. In this study, we further evaluated the performance of [^{18}F]VUIIS1009A and [^{18}F]VUIIS1009B in a preclinical model of neuroinflammation. PET imaging shows both radiotracers can be employed to detect the neuroinflammation region with a high SNR, as well as a fast distribution and equilibration in both contralateral and ipsilateral regions. In order to confirm further the binding specificity of [^{18}F]VUIIS109A and [^{18}F]VUIIS1009B for TSPO, we performed *in vivo* displacement assays by treating animals with unlabeled VUIIS1009A and VUIIS1009B during the 45-min dynamic scan. The result showed a high displacement ratio (up to 66%) for both radiotracers, which is almost the same to the ratio (up to 70%) reported by Martin *et al* for [^{18}F]DPA-714 displacement study using the same animal model[33], reflecting the high TSPO binding specificity for [^{18}F]VUIIS1009A/B.

Although [^{18}F]VUIIS1009A and [^{18}F]VUIIS1009B feature more than 500-fold enhancement of binding affinity when compared to [^{18}F]DPA-714, they did not demonstrate a superior semi-quantitative imaging profiles (%ID/cc) when compared with [^{18}F]DPA-714. Graphic analysis was also performed to determine the macro parameters (BP_{ND}, V_T and DVR) for these radiotracers in this study. The results demonstrate [^{18}F]VUIIS1009B has a higher V_T for both ipsilateral region and contralateral region, as well as higher BP_{ND}, V_T and DVR value when compared to [^{18}F]DPA-714, highlighting a superior performance to [^{18}F]DPA714. Parameter images (V_T and BP_{ND}) generated using Logan methods also demonstrate an enhanced visual effect for [^{18}F]VUIIS1009B when compared to [^{18}F]DPA-714. In pharmacokinetics, BP_{ND} is a combined measure of the density of "available" neuroreceptors and the affinity of a drug or radiotracer to that neuroreceptor. PET imaging performed in this study using the same rats with an equal TSPO density for each radiotracer. Consequently, BP_{ND} determined herein can reflect the binding affinities of the radiotracers and the sensitivity for TSPO density measurement. As expected, [^{18}F]VUIIS1009B demonstrates a much higher BP_{ND} than [^{18}F]DPA-714, as well as a strong correlation with BP_{ND} of [^{18}F]DPA-714 for both regional ROIs or at the voxel level. Moreover, slope of linearity is greater than one in **Figure 7**, reflecting [^{18}F]VUIIS1009B has the superior imaging potential and greater sensitivity to determine the TSPO expression in PET imaging when compared to [^{18}F]DPA-714. Correlation analysis was also performed for %ID/cc, BP_{ND} and V_T at the voxel level for each radiotracer, showing that all these three parameters has a strong correlation with each other for both [^{18}F]DPA-714 and [^{18}F]VUIIS1009B. Furthermore, [^{18}F]VUIIS1009B demonstrates a stronger positive linear relationship between V_T and BP_{ND} when compared to [^{18}F]DPA-714. This indicates [^{18}F]VUIIS1009B can be more accurately profiled than [^{18}F]DPA-714 using the AIFs based Logan and Logan reference tissue methods in this study. While for [^{18}F]VUIIS1009A, %ID/cc has a weaker correlation with both BP_{ND} and V_T as demonstrated in this study.

Furthermore, when compared to [^{18}F]DPA-714 and [^{18}F]VUIIS1009B, [^{18}F]VUIIS1009A does not demonstrate a higher BP_{ND} or DVR, which is also observed in our previous studies on C6 glioma imaging[17-18]. We believe this behavior is due to the higher plasma protein binding affinity of [^{18}F]VUIIS1009A when compared to [^{18}F]DPA-714 and [^{18}F]VUIIS1009B which was also noticed in our previous studies[18]. For [^{18}F]VUIIS1009A, the higher plasma protein binding affinity limits the partitioning of the radiotracer from blood to the tissues, and thus decreases its tissue uptake and image SNR, as well as the uptake of specific binding compartment, which will then impact the following macro parameter determination.

In this study, by evaluating two highly specific TSPO radiotracers [^{18}F]VUIIS1009A and [^{18}F]VUIIS1009B in a neuroinflammatory model, we aim to test and find a more sensitive radiotracer with superior macro parameters to reflect TSPO expression. Our present findings suggest that [^{18}F]VUIIS1009B will be a suitable PET radiotracer to fulfill this aim. We envision that [^{18}F]VUIIS1009B PET imaging coupled with parameter images (V_T and BP_{ND}) and graphic analysis (including Logan analysis and Reference Logan analysis) holds great promise for longitudinal neuroinflammation characterization. Although both [^{18}F]VUIIS1009B and [^{18}F]DPA-714 demonstrated a strong correlation between the semi quantitative parameter (%ID/cc) and the macro parameters (V_T, BP_{ND}) derived from the graphic analysis, further study still need to verify this correlation with the aim to decide which parameter should be employed for TSPO density evaluation under specific conditions. Besides that, further studies still need to be performed to clarify the binding specificities of [^{18}F]VUIIS1009A/B to different TSPO binders, which are produced in human as a result of *rs6971* single nucleotide polymorphism. Moreover, the pharmacokinetics and *in vivo* specific binding of [^{18}F]VUIIS1009A/B with TSPO, as well as the macro parameter-based analysis and images still need to be determined in the following primate studies.

Conclusion

This study focused on the radiosynthesis and evaluation of the novel TSPO probe [^{18}F]VUIIS1009A/B for neuroinflammation imaging in ischemic rats, using a series of *in vivo* assays and graphic analysis. The results of this study confirm that [^{18}F]VUIIS1009B PET imaging coupled with parameter images (V_T and BP_{ND}) and graphic analysis (both Logan and Reference Logan analysis) holds great promise for neuroinflammation characterization. We envision that [^{18}F]VUIIS1009B will be a suitable PET radiotracer for neuroinflammation imaging in many diseases.

Declarations

Ethics approval and consent to participate.

All applicable international, national, and institutional guidelines for the care and use of animals were followed.

Consent for publication.

Not applicable.

Availability of data and material.

The datasets used and/or analyzed during the current study are available from the corresponding author on reasonable request.

Competing interests.

The authors have declared that no competing interests exist.

Funding.

The study was supported by research grants from The National Science Foundation of China (Grant No. 81601536) by professor Dewei Tang.

Authors' contributions

Chen Huang: Experimental conception and design, data acquisition and analysis, manuscript drafting and revision.

Fan Ding: Data acquisition and analysis, manuscript drafting.

Yong Hao: Data acquisition, manuscript revision and data analysis.

Zhoumi Hu: Experimental conception, data acquisition and analysis.

Cheng Wang: Experimental conception, data acquisition and analysis .

Wei Li: Data acquisition and analysis.

Mengxin Wang: Data acquisition and analysis.

Wenxian Peng: Data acquisition and analysis, manuscript revision.

Dewei Tang: Experimental design, manuscript revision, approval of final content of manuscript.

Acknowledgements.

We would like to thank the staff at Renji Hospital and Huayi Isotopes Co. (Jiangsu, China) for their support with the cyclotron operation, radioisotope production, radiosynthesis, and animal experiments.

References

1. Albrecht DS, Granziera C, Hooker JM, Loggia ML. In Vivo Imaging of Human Neuroinflammation. ACS Chem Neurosci. 2016;7:470-83. doi:10.1021/acschemneuro.6b00056.
2. Airas L, Rissanen E, Rinne JO. Imaging neuroinflammation in multiple sclerosis using TSPO-PET. Clin Transl Imaging. 2015;3:461-73. doi:10.1007/s40336-015-0147-6.
3. Littlejohn G. Neurogenic neuroinflammation in fibromyalgia and complex regional pain syndrome. Nat Rev Rheumatol. 2015;11:639-48. doi:10.1038/nrrheum.2015.100.
4. Heppner FL, Ransohoff RM, Becher B. Immune attack: the role of inflammation in Alzheimer disease. Nat Rev Neurosci. 2015;16:358-72. doi:10.1038/nrn3880.
5. Crawshaw AA, Robertson NP. The role of TSPO PET in assessing neuroinflammation. J Neurol. 2017;264:1825-7. doi:10.1007/s00415-017-8565-1.
6. Dupont AC, Largeau B, Santiago Ribeiro MJ, Guilloteau D, Tronel C, Arlicot N. Translocator Protein-18 kDa (TSPO) Positron Emission Tomography (PET) Imaging and Its Clinical Impact in Neurodegenerative Diseases. Int J Mol Sci. 2017;18. doi:10.3390/ijms18040785.
7. Banati RB. Visualising microglial activation in vivo. Glia. 2002;40:206-17. doi:10.1002/glia.10144.
8. Dolle F, Luus C, Reynolds A, Kassiou M. Radiolabelled molecules for imaging the translocator protein (18 kDa) using positron emission tomography. Curr Med Chem. 2009;16:2899-923. doi:10.2174/092986709788803150.
9. Tang D, Hight MR, McKinley ET, Fu A, Buck JR, Smith RA, et al. Quantitative preclinical imaging of TSPO expression in glioma using N,N-diethyl-2-(2-(4-(2-18F-fluoroethoxy)phenyl)-5,7-dimethylpyrazolo[1,5-a]pyrimi din-3-yl)acetamide. J Nucl Med. 2012;53:287-94. doi:10.2967/jnumed.111.095653.
10. James ML, Fulton RR, Vercoullie J, Henderson DJ, Garreau L, Chalon S, et al. DPA-714, a new translocator protein-specific ligand: synthesis, radiofluorination, and pharmacologic characterization. J Nucl Med. 2008;49:814-22. doi:10.2967/jnumed.107.046151.
11. Corcia P, Tauber C, Vercoullie J, Arlicot N, Prunier C, Praline J, et al. Molecular imaging of microglial activation in amyotrophic lateral sclerosis. PLoS One. 2012;7:e52941. doi:10.1371/journal.pone.0052941.
12. Hamelin L, Lagarde J, Dorothee G, Leroy C, Labit M, Comley RA, et al. Early and protective microglial activation in Alzheimer's disease: a prospective study using 18F-DPA-714 PET imaging. Brain. 2016;139:1252-64. doi:10.1093/brain/aww017.
13. Golla SS, Boellaard R, Oikonen V, Hoffmann A, van Berckel BN, Windhorst AD, et al. Quantification of [18F]DPA-714 binding in the human brain: initial studies in healthy controls and Alzheimer's disease patients. J Cereb Blood Flow Metab. 2015;35:766-72. doi:10.1038/jcbfm.2014.261.
14. Ribeiro MJ, Vercouillie J, Debiais S, Cottier JP, Bonnaud I, Camus V, et al. Could (18) F-DPA-714 PET imaging be interesting to use in the early post-stroke period? EJNMMI Res. 2014;4:28. doi:10.1186/s13550-014-0028-4.
15. Medran-Navarrete V, Bernards N, Kuhnast B, Damont A, Pottier G, Peyronneau MA, et al. [18F]DPA-C5yne, a novel fluorine-18-labelled analogue of DPA-714: radiosynthesis and preliminary evaluation

as a radiotracer for imaging neuroinflammation with PET. J Labelled Comp Radiopharm. 2014;57:410-8. doi:10.1002/jlcr.3199.

16. Tang D, McKinley ET, Hight MR, Uddin MI, Harp JM, Fu A, et al. Synthesis and structure-activity relationships of 5,6,7-substituted pyrazolopyrimidines: discovery of a novel TSPO PET ligand for cancer imaging. J Med Chem. 2013;56:3429-33. doi:10.1021/jm4001874.
17. Tang D, Nickels ML, Tantawy MN, Buck JR, Manning HC. Preclinical imaging evaluation of novel TSPO-PET ligand 2-(5,7-Diethyl-2-(4-(2-[(18)F]fluoroethoxy)phenyl)pyrazolo[1,5-a]pyrimidin-3-yl)- N,N-diethylacetamide ([(18)F]VUIIS1008) in glioma. Mol Imaging Biol. 2014;16:813-20. doi:10.1007/s11307-014-0743-2.
18. Tang D, Li J, Buck JR, Tantawy MN, Xia Y, Harp JM, et al. Evaluation of TSPO PET Ligands [(18)F]VUIIS1009A and [(18)F]VUIIS1009B: Tracers for Cancer Imaging. Mol Imaging Biol. 2017;19:578-88. doi:10.1007/s11307-016-1027-9.
19. Wang L, Cheng R, Fujinaga M, Yang J, Zhang Y, Hatori A, et al. A Facile Radiolabeling of [(18)F]FDPA via Spirocyclic Iodonium Ylides: Preliminary PET Imaging Studies in Preclinical Models of Neuroinflammation. J Med Chem. 2017;60:5222-7. doi:10.1021/acs.jmedchem.7b00432.
20. Tang D, Li J, Nickels ML, Huang G, Cohen AS, Manning HC. Preclinical Evaluation of a Novel TSPO PET Ligand 2-(7-Butyl-2-(4-(2-[(18)F]Fluoroethoxy)phenyl)-5-Methylpyrazolo[1,5-a]Pyrimidin-3 -yl)-N,N-Diethylacetamide ((18)F-VUIIS1018A) to Image Glioma. Mol Imaging Biol. 2019;21:113-21. doi:10.1007/s11307-018-1198-7.
21. Tang D, Fujinaga M, Hatori A, Zhang Y, Yamasaki T, Xie L, et al. Evaluation of the novel TSPO radiotracer 2-(7-butyl-2-(4-(2-([(18)F]fluoroethoxy)phenyl)-5-methylpyrazolo[1,5-a]pyrimidin- 3-yl)-N,N-diethylacetamide in a preclinical model of neuroinflammation. Eur J Med Chem. 2018;150:1-8. doi:10.1016/j.ejmech.2018.02.076.
22. Wimberley C, Nguyen DL, Truillet C, Peyronneau MA, Gulhan Z, Tonietto M, et al. Longitudinal mouse-PET imaging: a reliable method for estimating binding parameters without a reference region or blood sampling. Eur J Nucl Med Mol Imaging. 2020. doi:10.1007/s00259-020-04755-5.
23. Rodriguez-Chinchilla T, Quiroga-Varela A, Molinet-Dronda F, Belloso-Iguerategui A, Merino-Galan L, Jimenez-Urbieta H, et al. [(18)F]-DPA-714 PET as a specific in vivo marker of early microglial activation in a rat model of progressive dopaminergic degeneration. Eur J Nucl Med Mol Imaging. 2020. doi:10.1007/s00259-020-04772-4.
24. Van Weehaeghe D, Babu S, De Vocht J, Zurcher NR, Chew S, Tseng CJ, et al. Moving towards multicenter therapeutic trials in ALS: feasibility of data pooling using different TSPO positron emission tomography (PET) radioligands. J Nucl Med. 2020. doi:10.2967/jnumed.119.241059.
25. Attwells S, Setiawan E, Rusjan PM, Xu C, Hutton C, Rafiei D, et al. Translocator Protein Distribution Volume Predicts Reduction of Symptoms During Open-Label Trial of Celecoxib in Major Depressive Disorder. Biol Psychiatry. 2020. doi:10.1016/j.biopsych.2020.03.007.
26. Fan Z, Dani M, Femminella GD, Wood M, Calsolaro V, Veronese M, et al. Parametric mapping using spectral analysis for (11)C-PBR28 PET reveals neuroinflammation in mild cognitive impairment

subjects. Eur J Nucl Med Mol Imaging. 2018;45:1432-41. doi:10.1007/s00259-018-3984-5.

27. Largeau B, Dupont AC, Guilloteau D, Santiago-Ribeiro MJ, Arlicot N. TSPO PET Imaging: From Microglial Activation to Peripheral Sterile Inflammatory Diseases? Contrast Media Mol Imaging. 2017;2017:6592139. doi:10.1155/2017/6592139.
28. Alves E, Bartlett PJ, Garcia CR, Thomas AP. Melatonin and IP3-induced Ca2+ release from intracellular stores in the malaria parasite Plasmodium falciparum within infected red blood cells. J Biol Chem. 2011;286:5905-12. doi:10.1074/jbc.M110.188474.
29. Peyronneau MA, Saba W, Goutal S, Damont A, Dolle F, Kassiou M, et al. Metabolism and quantification of [(18)F]DPA-714, a new TSPO positron emission tomography radioligand. Drug Metab Dispos. 2013;41:122-31. doi:10.1124/dmd.112.046342.
30. Logan J, Fowler JS, Volkow ND, Wang GJ, Ding YS, Alexoff DL. Distribution volume ratios without blood sampling from graphical analysis of PET data. J Cereb Blood Flow Metab. 1996;16:834-40. doi:10.1097/00004647-199609000-00008.
31. Lammertsma AA, Hume SP. Simplified reference tissue model for PET receptor studies. Neuroimage. 1996;4:153-8. doi:10.1006/nimg.1996.0066.
32. Rupprecht R, Papadopoulos V, Rammes G, Baghai TC, Fan J, Akula N, et al. Translocator protein (18 kDa) (TSPO) as a therapeutic target for neurological and psychiatric disorders. Nat Rev Drug Discov. 2010;9:971-88. doi:10.1038/nrd3295.
33. Martin A, Boisgard R, Theze B, Van Camp N, Kuhnast B, Damont A, et al. Evaluation of the PBR/TSPO radioligand [(18)F]DPA-714 in a rat model of focal cerebral ischemia. J Cereb Blood Flow Metab. 2010;30:230-41. doi:10.1038/jcbfm.2009.205.
34. Sacher C, Blume T, Beyer L, Peters F, Eckenweber F, Sgobio C, et al. Longitudinal PET Monitoring of Amyloidosis and Microglial Activation in a Second-Generation Amyloid-beta Mouse Model. J Nucl Med. 2019;60:1787-93. doi:10.2967/jnumed.119.227322.
35. Nguyen DL, Wimberley C, Truillet C, Jego B, Caille F, Pottier G, et al. Longitudinal positron emission tomography imaging of glial cell activation in a mouse model of mesial temporal lobe epilepsy: Toward identification of optimal treatment windows. Epilepsia. 2018;59:1234-44. doi:10.1111/epi.14083.
36. Beckers L, Ory D, Geric I, Declercq L, Koole M, Kassiou M, et al. Increased Expression of Translocator Protein (TSPO) Marks Pro-inflammatory Microglia but Does Not Predict Neurodegeneration. Mol Imaging Biol. 2018;20:94-102. doi:10.1007/s11307-017-1099-1.
37. Focke C, Blume T, Zott B, Shi Y, Deussing M, Peters F, et al. Early and Longitudinal Microglial Activation but Not Amyloid Accumulation Predicts Cognitive Outcome in PS2APP Mice. J Nucl Med. 2019;60:548-54. doi:10.2967/jnumed.118.217703.
38. Pulagam KR, Colas L, Padro D, Plaza-Garcia S, Gomez-Vallejo V, Higuchi M, et al. Evaluation of the novel TSPO radiotracer [(18)F] VUIIS1008 in a preclinical model of cerebral ischemia in rats. EJNMMI Res. 2017;7:93. doi:10.1186/s13550-017-0343-7.

39. Vainio SK, Dickens AM, Tuisku J, Eskola O, Solin O, Loyttyniemi E, et al. Cessation of anti-VLA-4 therapy in a focal rat model of multiple sclerosis causes an increase in neuroinflammation. EJNMMI Res. 2019;9:38. doi:10.1186/s13550-019-0508-7.
40. Golla SS, Boellaard R, Oikonen V, Hoffmann A, van Berckel BN, Windhorst AD, et al. Parametric Binding Images of the TSPO Ligand 18F-DPA-714. J Nucl Med. 2016;57:1543-7. doi:10.2967/jnumed.116.173013.

Table

Table 1. Macro Parameters determined for [^{18}F]DPA-714, [^{18}F]VUIIS1009A and [^{18}F]VUIIS1009B with the same cerebral ischemia rats (n = 6) (data = mean ± SD).

Probe	Ipsilateral (V_T)	Contralateral (V_T)	DVR_{Logan}	$DVR_{LoganRef}$	BP_{ND} (Ref. Logan)
[^{18}F]DPA-714	41.92 ± 7.91	6.94 ± 0.92	6.00 ± 0.41	5.37 ± 0.36	4.19 ± 0.10
[^{18}F]VUIIS1009A	28.93 ± 8.10	6.73 ± 2.14	4.37 ± 0.82	3.91 ± 0.50	2.90 ± 0.50
[^{18}F]VUIIS1009B	75.52 ± 6.53	9.23 ± 0.92	8.53 ± 1.06	7.55 ± 0.65	6.55 ± 0.65

Figures

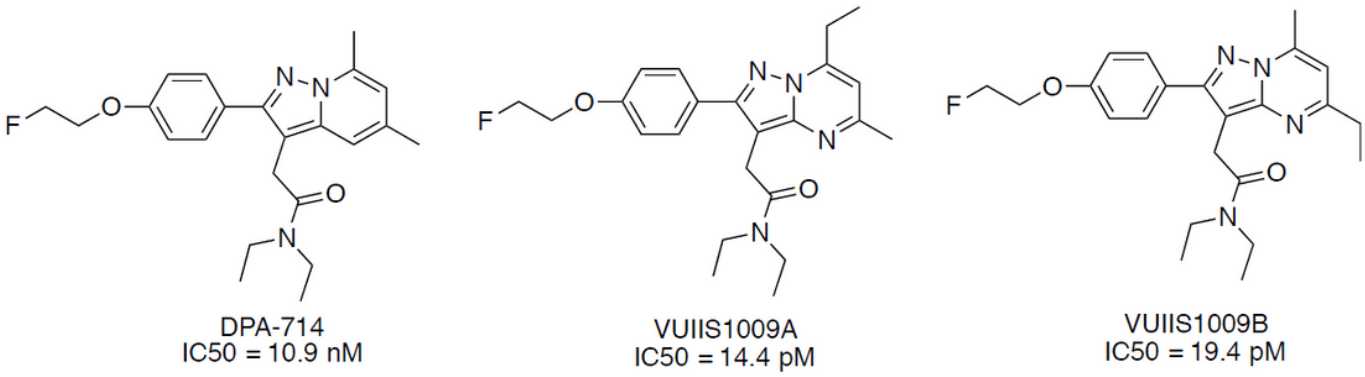

Figure 1

Structures of DPA-714, VUIIS1009A, VUIIS1009B and their corresponding IC50.

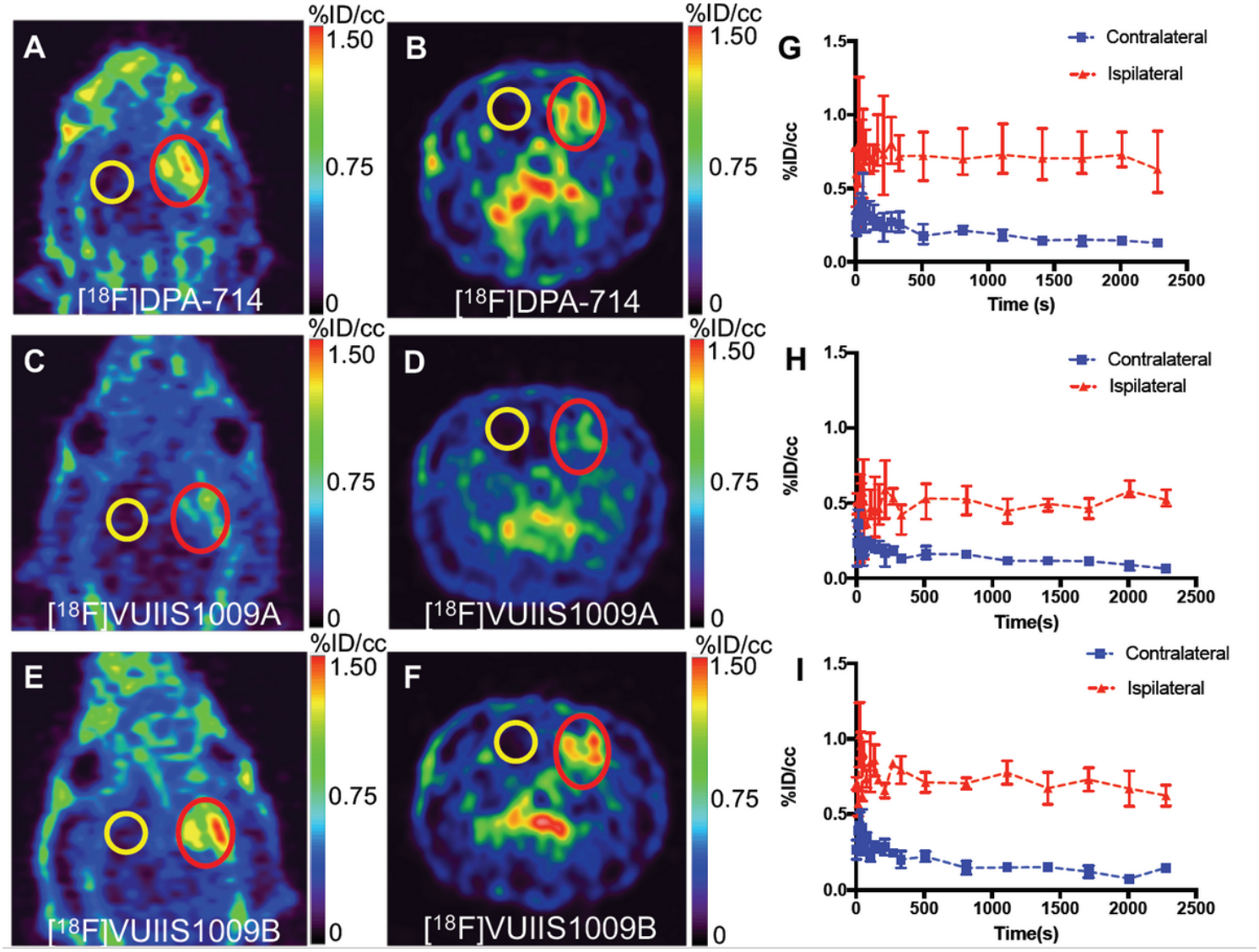

Figure 2

45-min PET dynamic scan for [18F]DPA-714, [18F]VUIIS1009A and [18F]VUIIS1009B. (a) Coronal and (b) transverse PET image of a cerebral ischemia rat from dynamic scan with [18F]DPA-714. (c) Coronal and (d) transverse PET image of the same cerebral ischemia rat from dynamic scan with [18F]VUIIS1009A. (e) Coronal and (f) transverse PET image of the same cerebral ischemia rat from dynamic scan with [18F]VUIIS1009B. Time activity curves (TACs) for the ipsilateral (red) and contralateral brain (blue) in the 45-min dynamic scan (n = 6) for [18F]DPA-714 (g), [18F]VUIIS1009A (h) and [18F]VUIIS1009A (f). %ID/cm3 = percentage injected dose per cubic centimeter. In TACs, data = mean ± SD. Ipsilateral ROI is marked by the red circle and contralateral ROI was marked by the yellow circle in the image.

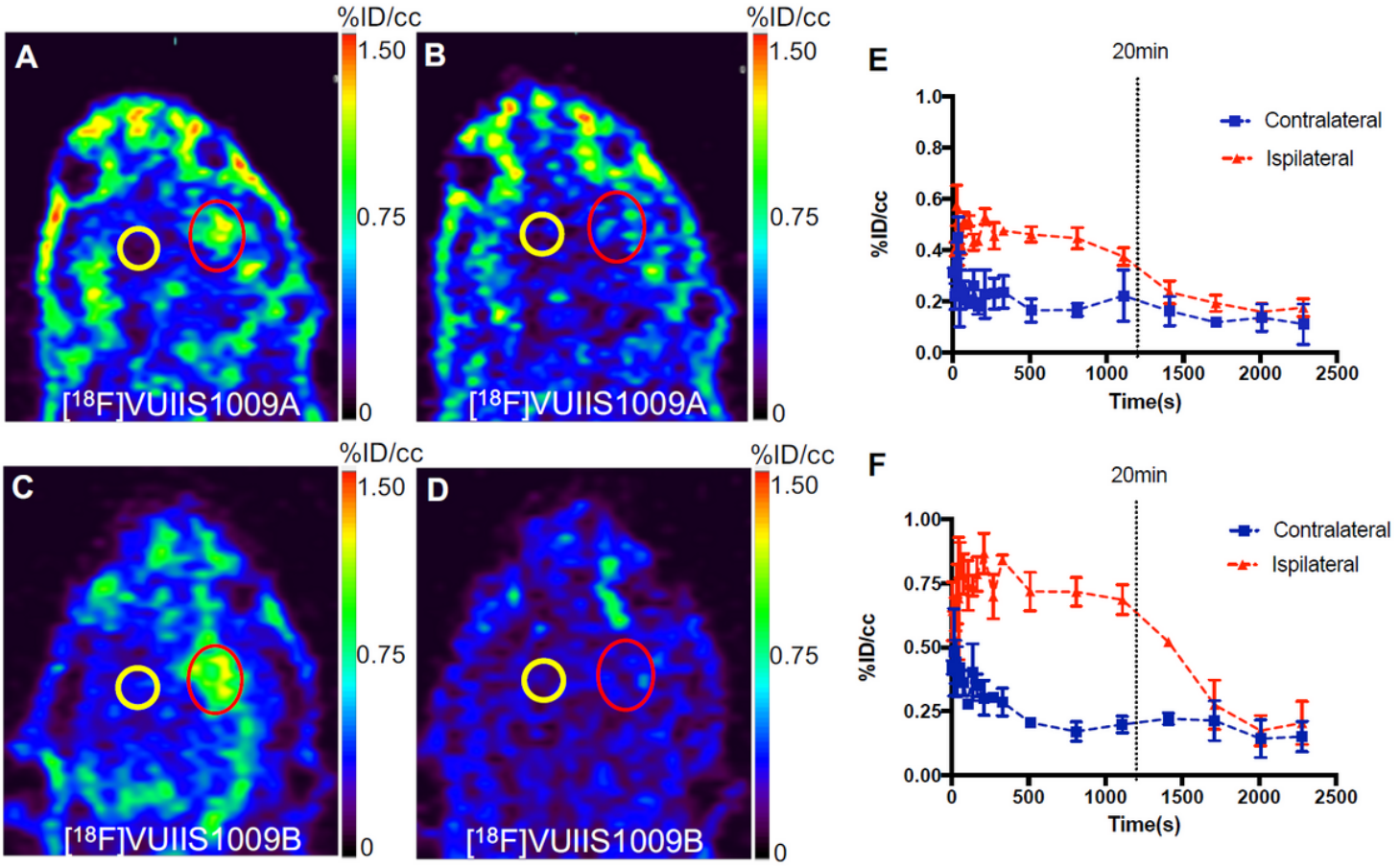

Figure 3

Displacement analysis for rats imaged by [18F]VUIIS1009A and [18F]VUIIS1009B with the injection of their corresponding non-radioactive analog (10 mg/kg) at 20 min. (a) Summation of the first 20 min PET imaging (coronal) with [18F]VUIIS1009A. (b) Summation of the last 25 min of PET imaging (coronal) with [18F]VUIIS1009A. (c) Ipsilateral and contralateral TACs for [18F]VUIIS1009A displacement analysis (n = 3). (d) Summation of the first 20 min of PET imaging (coronal) with [18F]VUIIS1009B (n = 3). (e) Summation of the last 25 min of PET imaging (coronal) with [18F]VUIIS1009B. (f) Ipsilateral and contralateral brain TACs for [18F]VUIIS1009B displacement analysis (n = 3). Ipsilateral ROI is marked with the red circle and contralateral ROI with yellow circle. Data = mean ± SD.

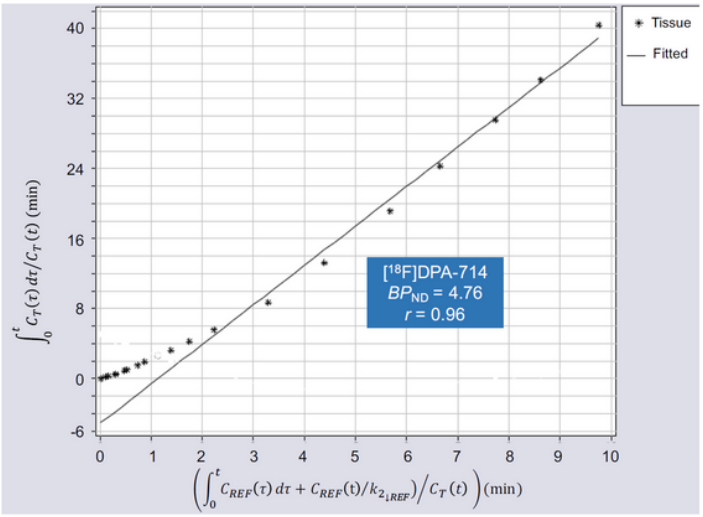

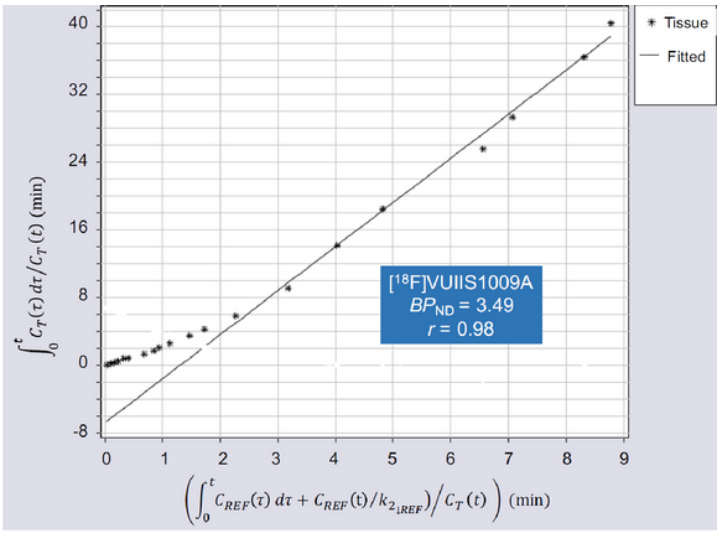

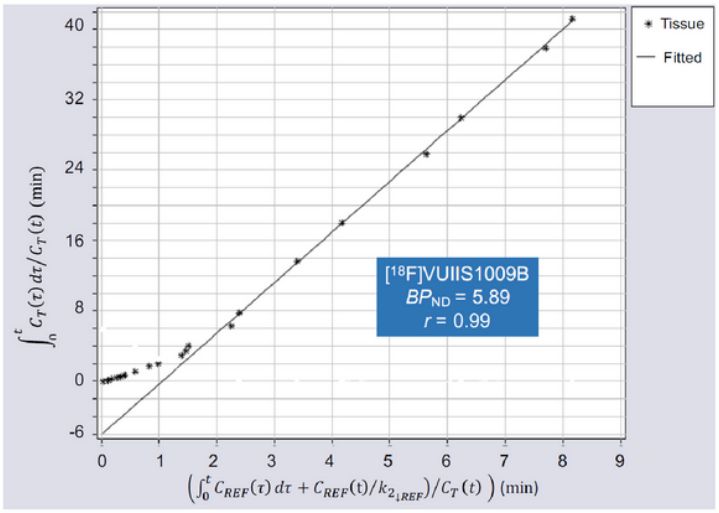

Figure 4

Graphic plot of the Logan Reference Tissue for (a)[18F]DPA-714, (b) [18F]VUIIS1009A and (c) [18F]VUIIS1009B.

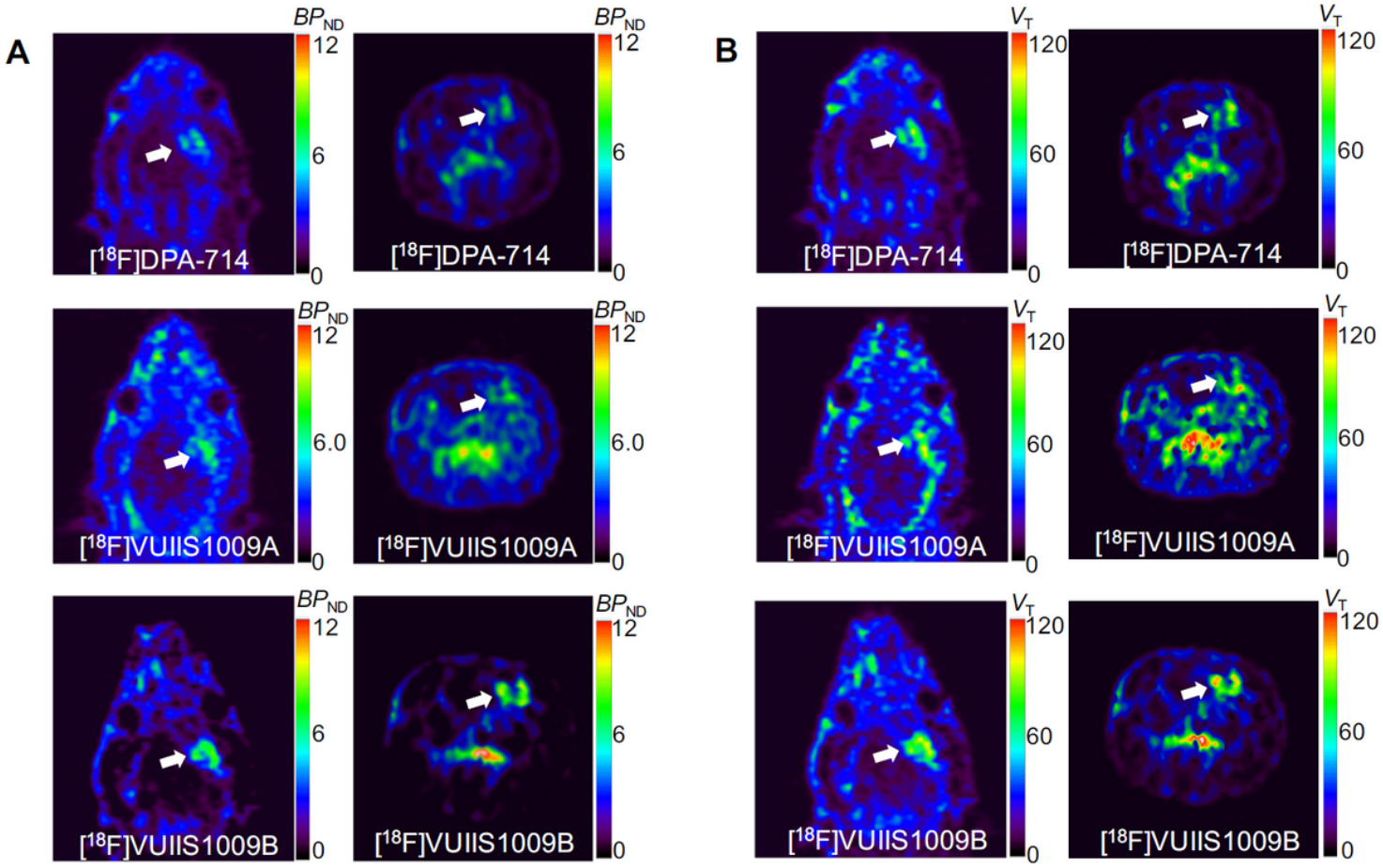

Figure 5

(a) Parametric images for [18F]DPA-714, [18F]VUIIS1009A and [18F]VUIIS1009B using Logan method with AIFs input. (b) Parametric images for [18F]DPA-714, [18F]VUIIS1009A and [18F]VUIIS1009B using Logan reference tissue method with TACs of the contralateral brain input as a reference region.

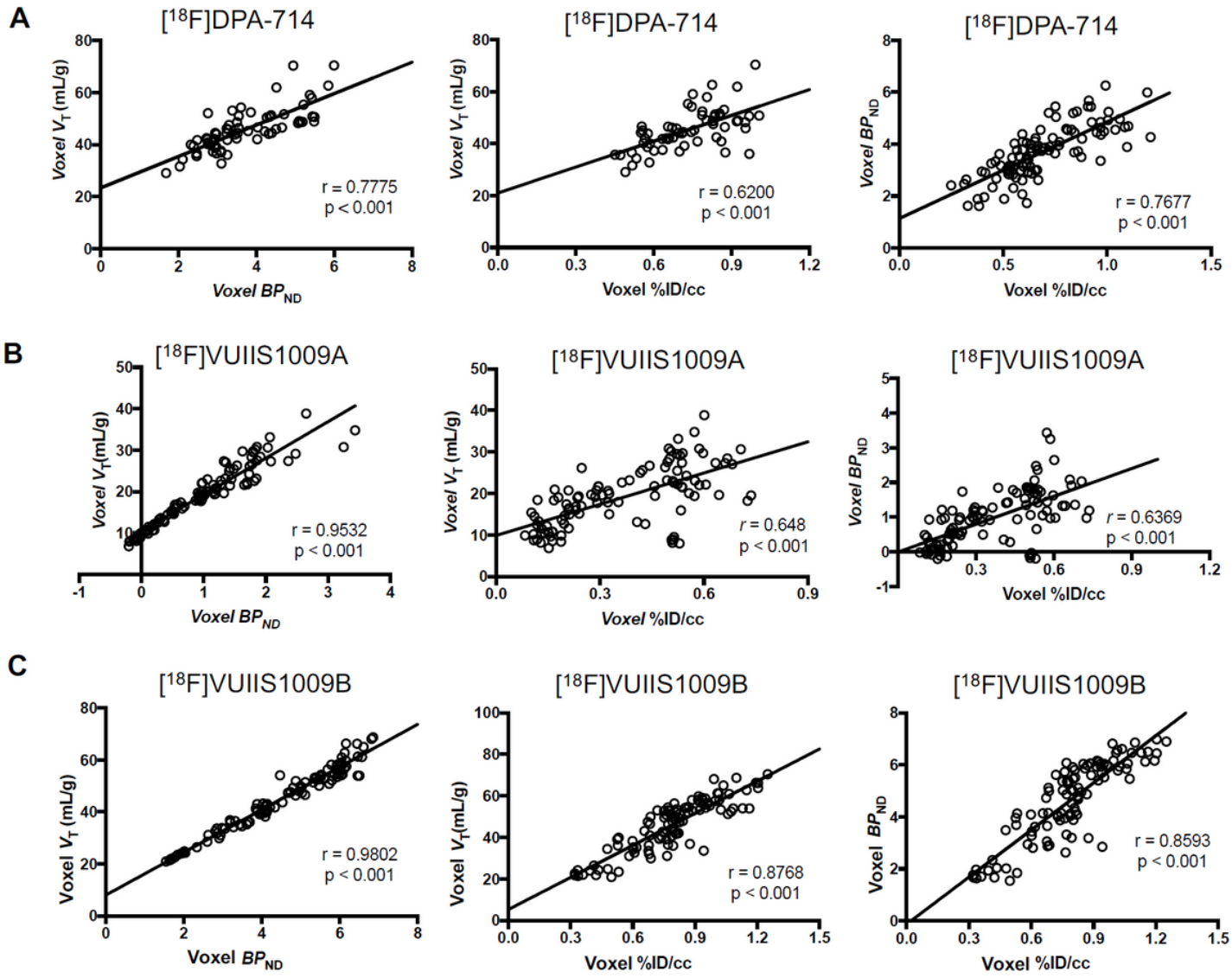

Figure 6

Correlation of %ID/cc, BPND and VT determined in this study for (a)[18F]DPA-714, (b)[18F]VUIIS1009A and (c)[18F]VUIIS1009B at voxel level. Dots (n = 60 to 80) indicates the voxels randomly collected from the ipsilateral brain in a cohort of rats (n = 6).

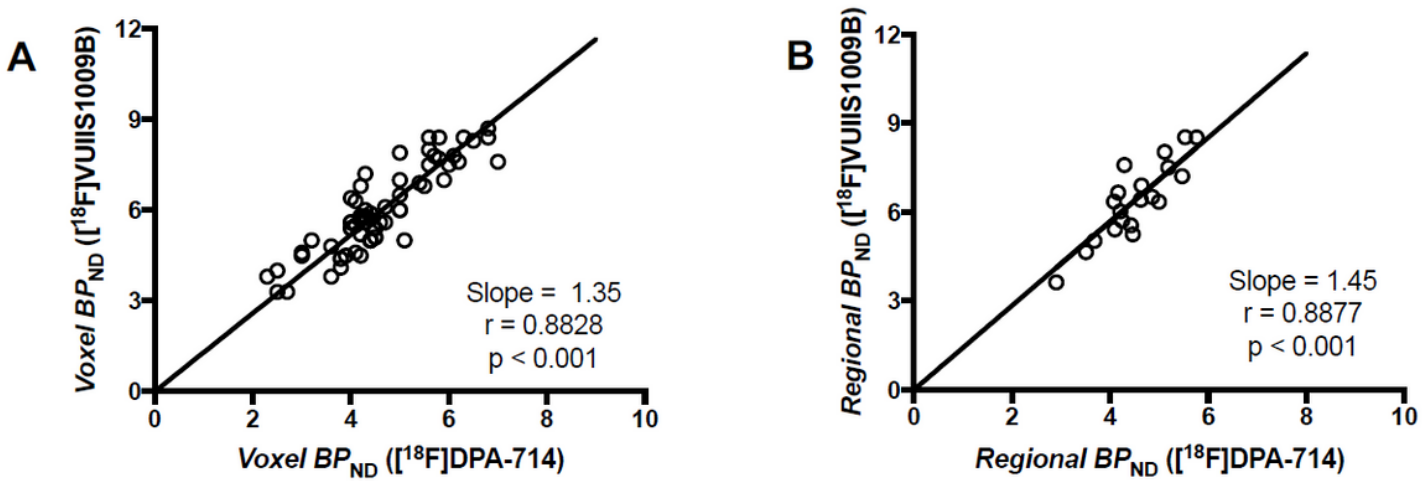

Figure 7

(a) Correlation of BPND determined from [18F]VUIIS1009B and [18F]DPA-714 dynamic PET scan in the same rats at the voxel level. Dots (n = 60) indicates the voxels randomly collected from the ipsilateral brain in a cohort of rats (n = 6). (b) Correlation of regional BPND determined from [18F]VUIIS1009B and [18F]DPA-714 dynamic PET scans in a cohort of rats (n = 6).

Supplementary Files

This is a list of supplementary files associated with this preprint. Click to download.

- SIfigs.pdf